Graphene coated ZnO nanowire optical waveguides

Bigeng Chen,[1] Chao Meng,[1] Zongyin Yang,[1] Wei Li,[1] Shisheng Lin,[2] Tingyi Gu,[3] Xin Guo,[1,4] Delong Wang,[1] Shaoliang Yu,[1] Chee Wei Wong,[3] and Limin Tong[1,*]

[1]*State Key Laboratory of Modern Optical Instrumentation, Department of Optical Engineering, Zhejiang University, Hangzhou 310027, China*

[2] *Department of Information Science and Electronic Engineering, Zhejiang University, Hangzhou 310027, China*

[3]*Optical Nanostructures Laboratory, Columbia University, New York, New York 10027, USA*

[4]*guoxin@zju.edu.cn*

**phytong@zju.edu.cn*

Abstract: We report the fabrication and characterization of freestanding graphene coated ZnO nanowires (GZNs) for optical waveguiding. The GZNs are fabricated using a tape-assist transfer under micromanipulation. Owing to the deep-subwavelength diameter and high index contrast of the ZnO nanowire waveguide, light-graphene interaction is significantly enhanced by the strong surface optical fields, resulting in a linear absorption as high as 0.11 dB/μm in a 606-nm-diameter GZN at 1550-nm wavelength. Launched by 1550-nm-wavelength femto-second pulses, a 475-nm-diameter GZN with a graphene coating length of merely 24 μm exhibits evident nonlinear saturable absorption with a peak power threshold down to 1.3 W. In addition, we also demonstrate a transmission modulation for 1550-nm-wavelength signal with a 590-nm-diameter GZN, showing the possibility of using GZN waveguides as nanoscale bulding blocks for nanophotonic devices.

OCIS codes: (230.7370) Waveguides; (050.6624) Subwavelength structures; (230.0230) Optical devices.

References and links

1. R. X. Yan, D. Gargas, and P. D. Yang, "Nanowire photonics," Nat. Photonics **3**(10), 569–576 (2009).
2. A. B. Greytak, C. J. Barrelet, Y. Li, and C. M. Lieber, "Semiconductor nanowire laser and nanowire waveguide electro-optic modulators," Appl. Phys. Lett. **87**(15), 151103 (2005).
3. M. A. Foster, A. C. Turner, M. Lipson, and A. L. Gaeta, "Nonlinear optics in photonic nanowires," Opt. Express **16**(2), 1300–1320 (2008).
4. F. X. Gu, H. K. Yu, W. Fang, and L. M. Tong, "Low-threshold supercontinuum generation in semiconductor nanoribbons by continuous-wave pumping," Opt. Express **20**(8), 8667–8674 (2012).
5. C. J. Barrelet, H. S. Ee, S. H. Kwon, and H. G. Park, "Nonlinear Mixing in Nanowire Subwavelength Waveguides," Nano Lett. **11**(7), 3022–3025 (2011).
6. R. Salem, M. A. Foster, A. C. Turner, D. F. Geraghty, M. Lipson, and A. L. Gaeta, "Signal regeneration using low-power four-wave mixing on silicon chip," Nat. Photonics **2**(1), 35–38 (2008).
7. G. P. Agrawal and N. A. Olsson, "Self-Phase Modulation and Spectral Broadening of Optical Pulses in Semiconductor Laser Amplifiers," IEEE J. Quantum Electron. **25**(11), 2297–2306 (1989).
8. T. L. Koch and R. A. Linke, "Effect of nonlinear gain reduction on semiconductor laser wavelength chirping," Appl. Phys. Lett. **48**(10), 613–615 (1986).
9. D. Van Thourhout, C. R. Doerr, C. H. Joyner, and J. L. Pleumeekers, "Observation of WDM Crosstalk in Passive Semiconductor Waveguides," IEEE Photon. Technol. Lett. **13**(5), 457–459 (2001).
10. D. Sun, Z. K. Wu, C. Divin, X. B. Li, C. Berger, W. A. de Heer, P. N. First, and T. B. Norris, "Ultrafast Relaxation of Excited Dirac Fermions in Epitaxial Graphene Using Optical Differential Transmission Spectroscopy," Phys. Rev. Lett. **101**(15), 157402 (2008).
11. R. Wu, Y. L. Zhang, S. C. Yan, F. Bian, W. L. Wang, X. D. Bai, X. H. Lu, J. M. Zhao, and E. G. Wang, "Purely Coherent Nonlinear Optical Response in Solution Dispersions of Graphene Sheets," Nano Lett. **11**(12), 5159–5164 (2011).
12. E. Hendry, P. J. Hale, J. Moger, A. K. Savchenko, and S. A. Mikhailov, "Coherent Nonlinear Optical Response of Graphene," Phys. Rev. Lett. **105**(9), 097401 (2010).
13. R. W. Boyd, *Nonlinear Optics* (Academic, 2008), Chap. 4.

#221151 - $15.00 USD Received 18 Aug 2014; revised 18 Sep 2014; accepted 18 Sep 2014; published 25 Sep 2014

14. Q. L. Bao and K. P. Loh, "Graphene Photonics, Plasmonics, and Broadband Optoelectronic Devices," ACS Nano **6**(5), 3677–3694 (2012).
15. K. S. Novoselov, A. K. Geim, S. V. Morozov, D. Jiang, M. I. Katsnelson, I. V. Grigorieva, S. V. Dubonos, and A. A. Firsov, "Two-dimensional gas of massless Dirac fermions in graphene," Nature **438**(7065), 197–200 (2005).
16. C. G. Lee, X. D. Wei, J. W. Kysar, and J. Hone, "Measurement of the Elastic Properties and Intrinsic Strength of Monolayer Graphene," Science **321**(5887), 385–388 (2008).
17. M. Liu, X. B. Yin, E. Ulin-Avila, B. S. Geng, T. Zentgraf, L. Ju, F. Wang, and X. Zhang, "A graphene-based broadband optical modulator," Nature **474**(7349), 64–67 (2011).
18. W. Li, B. G. Chen, C. Meng, W. Fang, Y. Xiao, X. Y. Li, Z. F. Hu, Y. X. Xu, L. M. Tong, H. Q. Wang, W. T. Liu, J. M. Bao, and Y. R. Shen, "Ultrafast All-Optical Graphene Modulator," Nano Lett. **14**(2), 955–959 (2014).
19. M. H. Huang, S. Mao, H. Feick, H. Q. Yan, Y. Y. Wu, H. Kind, E. Weber, R. Russo, and P. D. Yang, "Room-Temperature Ultraviolet Nanowire Nanolasers," Science **292**(5523), 1897–1899 (2001).
20. K. S. Kim, Y. Zhao, H. Jang, S. Y. Lee, J. M. Kim, K. S. Kim, J. H. Ahn, P. Kim, J. Y. Choi, and B. H. Hong, "Large-scale pattern growth of graphene films for stretchable transparent electrodes," Nature **457**(7230), 706–710 (2009).
21. Y. F. Hao, Y. Y. Wang, L. Wang, Z. H. Ni, Z. Q. Wang, R. Wang, C. K. Koo, Z. X. Shen, and J. T. L. Thong, "Probing Layer Number and Stacking Order of Few-Layer Graphene by Raman Spectroscopy," Small **6**(2), 195–200 (2010).
22. A. C. Ferrari, J. C. Meyer, V. Scardaci, C. Casiraghi, M. Lazzeri, F. Mauri, S. Piscanec, D. Jiang, K. S. Novoselov, S. Roth, and A. K. Geim, "Raman Spectrum of Graphene and Graphene Layers," Phys. Rev. Lett. **97**(18), 187401 (2006).
23. L. M. Tong, R. R. Gattass, J. B. Ashcom, S. L. He, J. Y. Lou, M. Y. Shen, I. Maxwell, and E. Mazur, "Subwavelength-diameter silica wires for low-loss optical wave guiding," Nature **426**(6968), 816–819 (2003).
24. B. Yan, L. Liao, Y. M. You, X. J. Xu, Z. Zheng, Z. X. Shen, J. Ma, L. M. Tong, and T. Yu, "Single-Crystalline V_2O_5 Ultralong Nanoribbon Waveguides," Adv. Mater. **21**(23), 2436–2440 (2009).
25. Y. G. Ma, X. Y. Li, H. K. Yu, L. M. Tong, Y. Gu, and Q. H. Gong, "Direct measurement of propagation losses in silver nanowires," Opt. Lett. **35**(8), 1160–1162 (2010).
26. Y. Chen, Z. Ma, Q. Yang, and L. M. Tong, "Compact optical short-pass filters based on microfibers," Opt. Lett. **33**(21), 2565–2567 (2008).
27. Q. Ye, J. Wang, Z. B. Liu, Z. C. Deng, X. T. Kong, F. Xing, X.-D. Chen, W.-Y. Zhou, C.-P. Zhang, and J.-G. Tian, "Polarization-dependent optical absorption of graphene under total internal reflection," Appl. Phys. Lett. **102**(2), 021912 (2013).
28. R. R. Nair, P. Blake, A. N. Grigorenko, K. S. Novoselov, T. J. Booth, T. Stauber, N. M. R. Peres, and A. K. Geim, "Fine Structure Constant Defines Visual Transparency of Graphene," Science **320**(5881), 1308 (2008).
29. Y. G. Ma, X. Guo, X. Q. Wu, L. Dai, and L. M. Tong, "Semiconductor nanowire lasers," Adv. Opt. Photon. **5**(3), 216–273 (2013).
30. Q. L. Bao, H. Zhang, Y. Wang, Z. H. Ni, Y. L. Yan, Z. X. Shen, K. P. Loh, and D. Y. Tang, "Atomic-Layer Graphene as a Saturable Absorber for Ultrafast Pulsed Lasers," Adv. Funct. Mater. **19**(19), 3077–3083 (2009).
31. H. Z. Yang, X. B. Feng, Q. Wang, H. Huang, W. Chen, A. T. S. Wee, and W. Ji, "Giant Two-Photon Absorption in Bilayer Graphene," Nano Lett. **11**(7), 2622–2627 (2011).
32. Z. B. Liu, M. Feng, W. S. Jiang, W. Xin, P. Wang, Q. W. Sheng, Y. G. Liu, D. N. Wang, W. Y. Zhou, and J. G. Tian, "Broadband all-optical modulation using a graphene-covered-microfiber," Laser Phys. Lett. **10**(6), 065901 (2013).
33. J. Svensson, N. Anttu, N. Vainorius, B. M. Borg, and L. E. Wernersson, "Diameter-Dependent Photocurrent in InAsSb Nanowire Infrared Photodetectors," Nano Lett. **13**(4), 1380–1385 (2013).

1. Introduction

As one-dimensional active nanomaterials with uniform geometries and high refractive indices, semiconductor nanowires (NWs) have intrigued considerable attention in constructing nanoscale photonic components and devices such as waveguides, lasers and modulators [1,2]. For subwavelength waveguiding, the semiconductor NW offers some favorable properties such as tight optical confinement and highly engineerable waveguide dispersion for strengthening light-material interaction on a miniaturized footprint [3], leading to significantly enhanced nonlinear effects that have found wide applications ranging from supercontinuum generation, wavelength conversion to signal regeneration [4–6]. However, nonlinear effects in semiconductor without rational control will also possibly lead to detrimental influences on device performances like frequency chirping, waveform distortion and signal crosstalk [7–9]. Besides, different nonlinear processes may also arise simultaneously and interact with each other in a single NW [4], making it difficult to select a particular nonlinear functionality. Recently, graphene was reported to exhibit a variety of exceptional optical properties. The relaxation of photo-excited carriers lasts for only a few pico-seconds [10], while the third-order susceptibility is several orders of magnitude greater than that of semiconductor at

#221151 - $15.00 USD Received 18 Aug 2014; revised 18 Sep 2014; accepted 18 Sep 2014; published 25 Sep 2014

visible and near-IR wavelengths [11–13]. In addition, graphene presents large band-filling related nonlinearity in an ultrawide spectral region (from visible to mid-IR) due to strong interband transition [14,15]. Being atomically thin and mechanically robust [16], it is also highly flexible to be incorporated into other micro/nanophotonic structures [17,18]. Here we demonstrate a graphene coated ZnO NW (GZN) optical waveguide combining excellent waveguiding properties of NWs and ultrahigh optical nonlinearity of graphene. The freestanding GZN was fabricated by transferring a few-layer graphene flake onto a ZnO NW synthesized via chemical vapor transport process, and dissolving the tape supporting the graphene flake afterward. Using a fiber-taper-assistant near-field-coupling technique, light was efficiently launched into and waveguided through the GZN with a linear absorption of 0.11 dB/μm contributed by the graphene coat. By measuring the input-power-dependent transmission of the GZN using femto-second pulses (1064- and 1550-nm wavelength, respectively), we observed band-filling induced saturable absorption (SA) raised from the graphene-light interaction along the length of the GZN, which was significantly enhanced due to the tightly confined optical fields of the guiding mode on the surface of the high-index subwavelength-diameter GZN. When waveguiding 1550-nm-wavelength femtosecond pulses in a 24-μm-length GZN, we further demonstrated a differential transmission (DT) of 11% with SA threshold power down to 1.3 W, which is much lower than the graphene coated microfiber owing to the much tighter optical confinement of the ZnO nanowire [18]. In addition, as an example for nonlinear nanophotonic applications, we demonstrated optical modulation of a 1550-nm-wavelength signal using these deep-subwavelength GZNs.

2. Fabrication of graphene coated ZnO nanowires

The fabrication of a GZN is schematically illustrated in Fig. 1. Firstly a few-layer graphene flake was exfoliated from a kish graphite sample by a scotch tape and left on the tape. A ZnO NW, synthesized via a chemical vapor transport process, was placed across the graphene flake via micromanipulation (Fig. 1(a)). Secondly, the tape was pasted onto a Si/SiO_2 wafer (300 nm SiO_2), with the side that contained the NW facing down (Fig. 1(b)). Thirdly, the wafer was immersed into a 4-methyl-2-pentanone solution at 70 °C. When the tape was completely dissolved after about 10 minutes, a graphene-covered NW was left on the wafer (Fig. 1(c)). Then, a nano-second pulsed laser beam through a nanoscale silica fiber taper was employed to cut apart the graphene along both sides of the NW on the wafer (Fig. 1(d)). Finally, the NW was lifted up from the wafer (Fig. 1(e)) and the graphene spontaneously wrapped around the NW to form a GZN. Figure 1(f) shows a typical optical micrograph of an as-fabricated GZN, with the ZnO NW of about 600 nm in diameter and 80 μm in length.

#221151 - $15.00 USD Received 18 Aug 2014; revised 18 Sep 2014; accepted 18 Sep 2014; published 25 Sep 2014

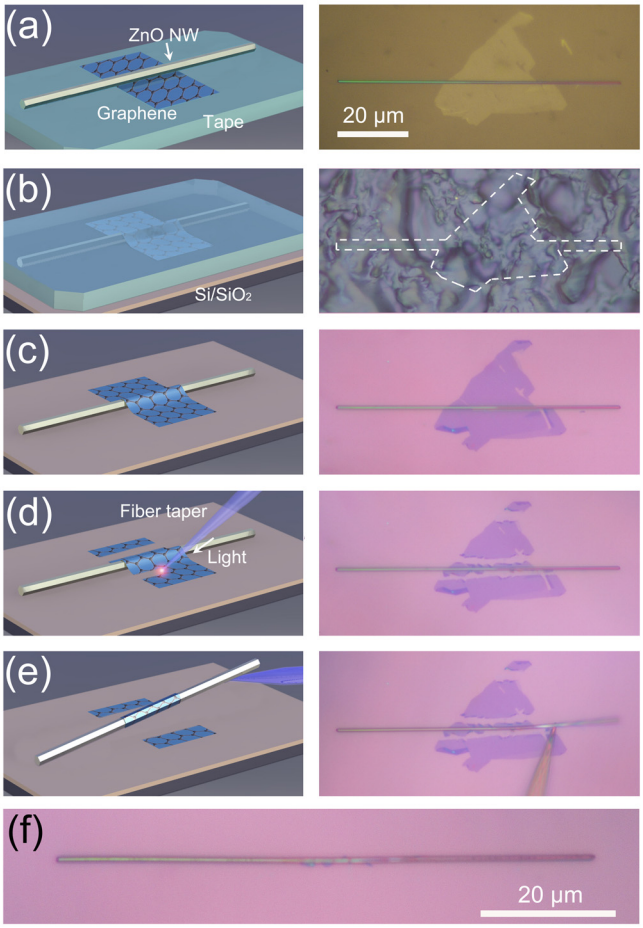

Fig. 1. Schematic diagrams and corresponding optical micrographs of the GZN fabrication. (a) A ZnO NW was placed across a few-layer graphene flake attached on a scotch tape via micromanipulation. (b) The tape with the graphene and the NW was pasted on a Si/SiO_2 wafer. (c) After the tape was dissolved in a 4-methyl-2-pentanone solution, the graphene-covered NW was left on the wafer. (d) The graphene on the wafer was cut along the NW by nano-second laser pulses introduced by a fiber taper. (e) The NW was lifted up with the graphene by the fiber taper. f) An as-fabricated GZN with the ZnO NW of about 600 nm in diameter and 80 μm in length. The scale bar in (a) is also applicable to (b-e).

The morphology of the GZN was examined by scanning electron microscopy (SEM), as depicted in Fig. 2(a)-(c). Figure 2(a) gives a SEM image of a 540-nm-diameter GZN, showing excellent diameter uniformity and surface smoothness of the ZnO NW. From the close-up images of the graphene-coated areas (Fig. 2(b) and 2(c)), it is clear to see that the NW is coated tightly by the graphene with a few wrinkles. For better resolution, we used high-resolution transmission electron microscopy (HRTEM) to characterize the crystal structure of the GZN. Figure 2(d) gives a typical HRTEM image of a sidewall area of the GZN, where the lattice-fringe along the axial direction of the ZnO NW and layer structure of the graphene are both shown clearly. The lattice-fringe separation is 0.26 nm conformed to the lattice parameter of the c-axis of wurtzite ZnO NWs [19]. The out of plane lattice parameter of the few-layer graphene is 0.35 nm, which agrees with the previous result [20]. Figure 2(e) shows microscopic Raman spectra of graphene flakes coated on two GZNs. The fitted widths of the 2D peaks (centered at around 2700 cm^{-1}) 50.2 cm^{-1} (black line) and 57.4 cm^{-1} (red line) reveal that the graphene coats of the two GZNs are bilayer and trilayer, respectively [21]. Besides, the defect-induced D peaks (around 1350 cm^{-1}) are negligible [22], indicating the

#221151 - $15.00 USD Received 18 Aug 2014; revised 18 Sep 2014; accepted 18 Sep 2014; published 25 Sep 2014

high quality of the graphene layers. Generally, the graphene coat of a GZN has a uniform layer-number as the fabrication is started with one homogeneous graphene flake attached on the scotch tape (Fig. 1(a)). At the same time, we can also fabricate a GZN coated with multiple different graphene layers. A Raman mapping for the intensity ratios of G peaks to 2D peaks from three GZNs with their optical micrograph are given by Fig. 2(f) and 2(g). where the GZN(ii) is coated by one monolayer flake (I_G: I_{2D} <1) and two multi-layer flakes. This is realized by placing the ZnO NW across three graphene flakes with different layer-numbers on the tape.

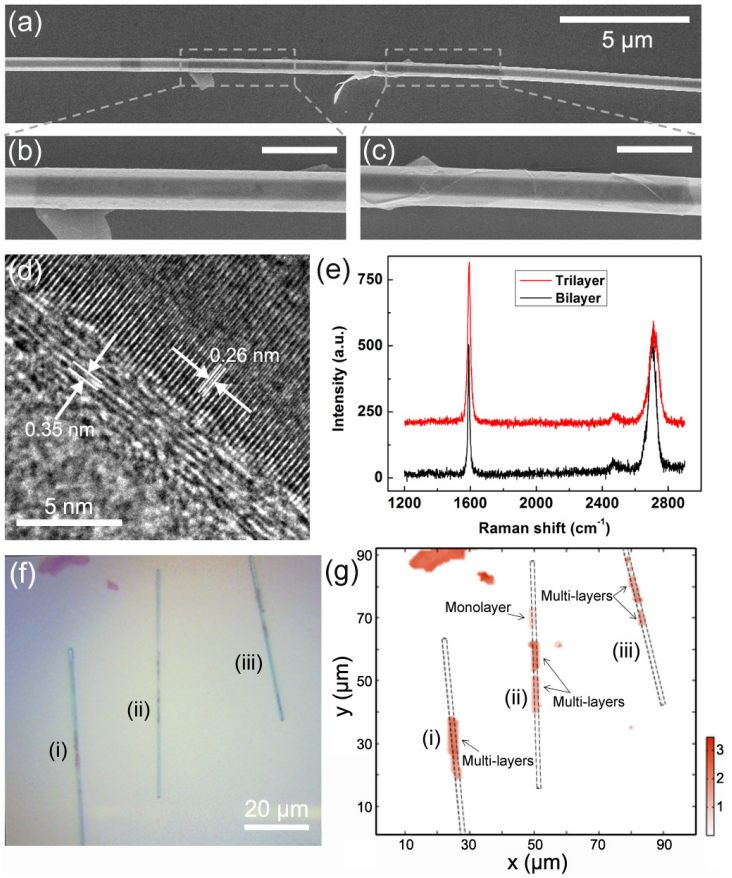

Fig. 2. Electron microscope and Raman spectrum characterizations of GZNs. (a-c) SEM images of a 540-nm-diameter GZN. (b) and (c) show the close-up views of the two grey dashed boxes in (a) with the scale bars of 1μm. (d) TEM image of a sidewall area on the GZN. (e) Raman spectra of two GZNs coated by bilayer and trilayer graphene. (f-g) Optical micrograph of three GZNs and the corresponding Raman mapping for the intensity ratios of G peaks to 2D peaks. The dotted boxes in (g) correspond to the outlines of the GZNs. The upper left of the images show two graphene flakes on the substrate.

3. Linear optical characterization of GZNs

To evaluate the linear propagation loss coefficient of the GZN at 1550 nm, we employed a propagation-distance-dependent output measurement that has been widely used for optical characterization of nanowire waveguides [23–25]. As shown in Fig. 3(a) and 3(b), a 606-nm-diameter GZN with a trilayer graphene coat was suspended across a Si/SiO_2 microchannel to avoid substrate-induced leakage [26]. To obtain the propagation-distance-dependent output at 1550 nm, we moved the launching fiber taper along the length of the GZN, and recorded the output intensity from the other end of the GZN using a collection fiber taper (Fig. 3(a) and

#221151 - $15.00 USD Received 18 Aug 2014; revised 18 Sep 2014; accepted 18 Sep 2014; published 25 Sep 2014

3(b)), with measured results given in Fig. 3(c) (circles and squares). To maintain an almost constant input coupling efficiency, we carefully adjusted the angle and position of the launching taper until the coupling is optimized with maximum output, and then horizontally moved the launching taper along the GZN without changing the contact angle [25]. The input power of the 1550-nm CW light was 100 μW. Using a exponential decay function fitting method, we obtained propagation loss coefficients of 0.15 dB/μm at the graphene coated section and 0.04 dB/μm for the uncoated section respectively, revealing the linear absorption of the graphene coat to be about 0.11 dB/μm. The large absorption of the graphene coat was mainly due to tightly confined waveguiding scheme and the enhanced optical field around the surface of the GZN. In a previous report, the absorption of graphene demonstrated obvious polarization dependence under a total internal reflection scheme [27]. However, because of the much longer light-graphene interaction length (~40μm, which means a large number of interaction times) and a nearly 360° coating around the surface of the GZN, the absorption measured in this work can be roughly considered polarization-independent. Also, since the optical absorption of graphene is proportional to the layer number N when $N \leq 4$ [28], the propagation loss of a GZN with different N ($N \leq 4$) can be estimated from the loss obtained here. The propagation loss coefficient of the uncoated ZnO section is higher than those in previous report [1], which probably arise from larger scattering loss caused by surface contamination or imperfection at longer wavelength. As for 633-nm wavelength, the measured propagation loss coefficient of the ZnO fell to 0.004 dB/μm. Figure 3(d) shows the calculated power density distribution on the cross-section plane of a 600-nm-diameter ZnO NW waveguiding a 1-W 1550-nm-wavelength light in a HE_{11}-like mode [29] with radial power density (along the dotted line in Fig. 3(d)) depicted in Fig. 3(e). Due to the small diameter, the NW can only support two HE_{11}-like modes with perpendicular polarizations. It is noticeable that, the power density on the surface of the NW is about 150 MW/cm^2 under the 1-W input.

#221151 - $15.00 USD Received 18 Aug 2014; revised 18 Sep 2014; accepted 18 Sep 2014; published 25 Sep 2014

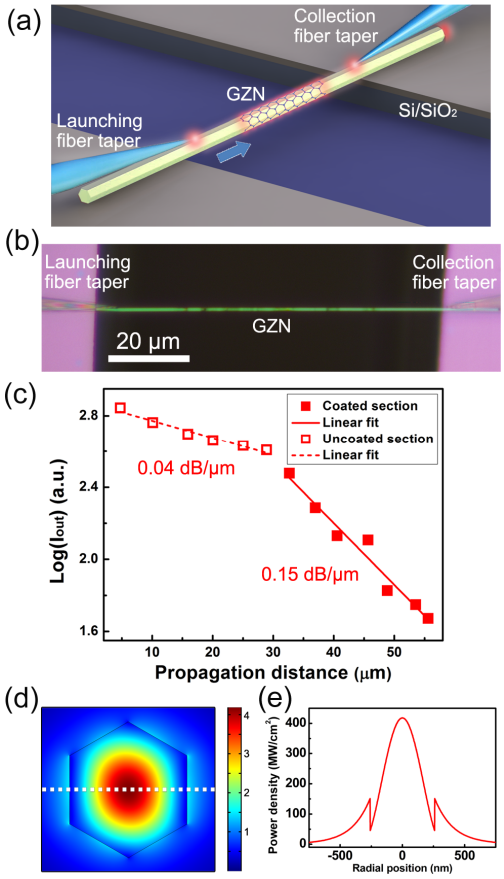

Fig. 3. Propagation loss characterization of a 606-nm-diameter GZN and calculated power density distribution on the cross-section of a ZnO NW at 1550-nm wavelength. (a-b) Schematic diagram and optical micrograph of the experimental setup for propagation loss measurement of the GZN. (c) Propagation-distance-dependent output intensity of the GZN. The solid and dash lines are the linear fits for the experimental data of the coated section and uncoated section on the GZN respectively. (d) Power density distribution on the cross-section of an air-clad 600-nm-diameter ZnO NW calculated by COMSOL. Here the diameter is defined as the distance between two opposite vertices of the hexagonal cross-section. (e) Power density dependence along the dotted line in (d) on the radial position with 1-W CW input.

4. Nonlinear optical characterization of GZNs

The nonlinear response of the GZN was investigated by measuring the input-power-dependent transmission with 1064- and 1550-nm wavelength femto-second pulses (76MHz, 220 fs) input. Figure 4(a) gives the schematic diagram of the measurement setup. A 1 × 2 fiber coupler was employed to monitor the input power in real time. The laser beam was firstly split into two by a 1 × 2 fiber coupler: one beam was used as the reference (measured by the power meter A), and the other was coupled into a freestanding GZN by a fiber taper and worked as a probing light. The output of the GZN was collected by another fiber taper and measured by the power meter B. By comparing the total propagation loss (including both the in- and out-coupling losses between the GZN and the fiber tapers) and the propagation loss of the GZN, we obtained an efficiency of about 64% for a single in- or out-coupling between the fiber taper and the GZN, and determined the power coupled into the GZN at its input end. Figure 4(b) shows the normalized input-power-dependent transmissions of a 475-nm-diameter GZN with a 24-μm-long trilayer graphene coat at 1064- and 1550-nm wavelength (solid symbols), respectively. For comparison, the normalized input-power-dependent transmission of a 490-

#221151 - $15.00 USD Received 18 Aug 2014; revised 18 Sep 2014; accepted 18 Sep 2014; published 25 Sep 2014

nm-diameter ZnO NW without graphene coat was also provided (open symbols). The transmission of the GZN at 1550 nm increases rapidly as the input peak power exceeds 1.3 W and saturates at 4.5 W with a DT of 11% (solid squares). At 1064 nm the GZN also demonstrates a similar nonlinear transmission (solid circles) with a SA threshold power of 2.7 W. The rapid increase and saturation behaviors of the transmission had been explained from the aspect of graphene ultrafast carrier dynamics in previous studies [10,30].Within the power range of the measurement, nonlinear transmissions are hardly observed in the ZnO NW at both two wavelengths (open squares for 1550 nm and open circles for 1064 nm). Figure 4(c) shows the output spectra of the GZN with 1064- and 1550-nm input and 10-W peak power (corresponding to a surface power density of 1.5 GW/cm^2 for 1064-nm and 0.8 GW/cm^2 for 1550-nm light, respectively). With both inputs, only the input light is observed, indicating that under the power densities and the nanowire length used here, excepting the SA of graphene, nonlinear effects of both graphene and ZnO such as second or third harmonic generation are negligible. Owing to the large bandgap of the ZnO NW (3.37 eV) and the high intensity requirement for two-photon absorption of graphene [19,31], the two-photon absorption was also suppressed in the GZN. In addition, compared to the normal-incidence scheme for the studies of graphene's SA in previous reports [10,30], the waveguiding scheme of the GZN demonstrated here provides greatly enhanced graphene-light interaction in both field intensity and interaction length, thus contributing to more pronounced SA effect and larger DTs.

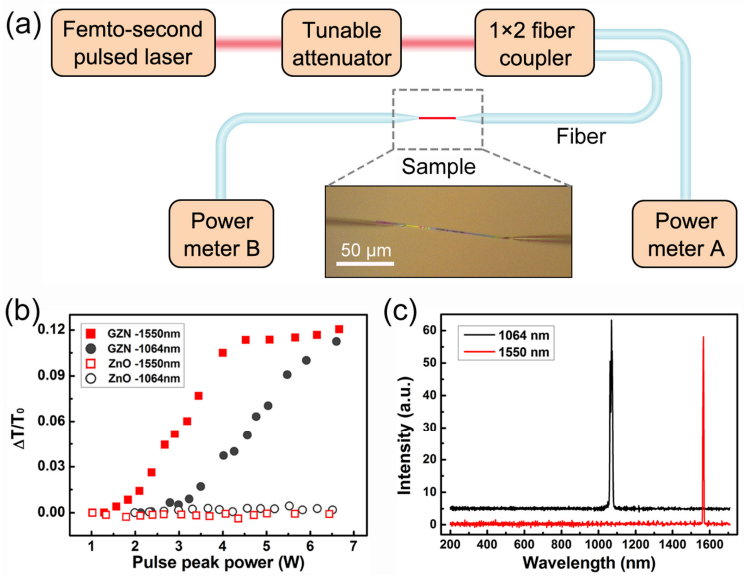

Fig. 4. Input-power-dependent transmission measurement of a 475-nm-diameter GZN. (a) Schematic diagram of the measurement setup. (b) Input-power-dependent transmissions of the GZN at 1064- and 1550-nm wavelengths, respectively. A transmission of a 490-nm-diameter ZnO is also given for comparison. (c) Output spectra of the GZN.

5. Optical modulation with GZNs

The above-mentioned SA effect offers the possibility for modulating transmission of the GZN using an all-optical scheme [18,32]. As an example, we used nano-second pump pulses to switch out signal pulses waveguided in a 590-nm-diameter GZN (Fig. 5(a)). A 1550-nm CW signal light was waveguided through the GZN with a low transmission. When 1064-nm nano-second laser pulses (~8 ns, 2.4 kHz) were sent through the GZN with an average power of 120 μW (peak power 6.2 W, surface power density 0.6 GW/cm^2), the transmission of the CW signal light was increased temporary due to the SA during the presence of the switch pulses, resulting in evident optical modulation of the signal with a repetition identical to that of the pulsed laser (red curve in Fig. 5(b)). With switch light on, when the signal light is turned off,

#221151 - $15.00 USD Received 18 Aug 2014; revised 18 Sep 2014; accepted 18 Sep 2014; published 25 Sep 2014

the modulation feature disappeared (black background in Fig. 5(b)), confirming that the pulses is originated from the modulated signal light. The relatively slow response of the optical modulation (~24-μs rising and ~113-μs falling of a switched signal pulse) is contributed by the parasite electronic response of the photodetector and the oscilloscope. The principle of the modulation is illustrated in Fig. 5(c). The weak 1550-nm signal light coupled into the GZN experiences significant attenuation due to absorption in graphene as it propagates along. When the 1064-nm switch light is introduced, it excites carriers in the graphene, and through Pauli blocking of interband transitions, reducing the absorption of graphene to the 1550-nm light, resulting in evident modulation of the signal output from the GZN. Although the modulation depth is relatively low, our experimental results shown here indicate the potential of using GZNs for all-optical modulation on the micro/nanoscale.

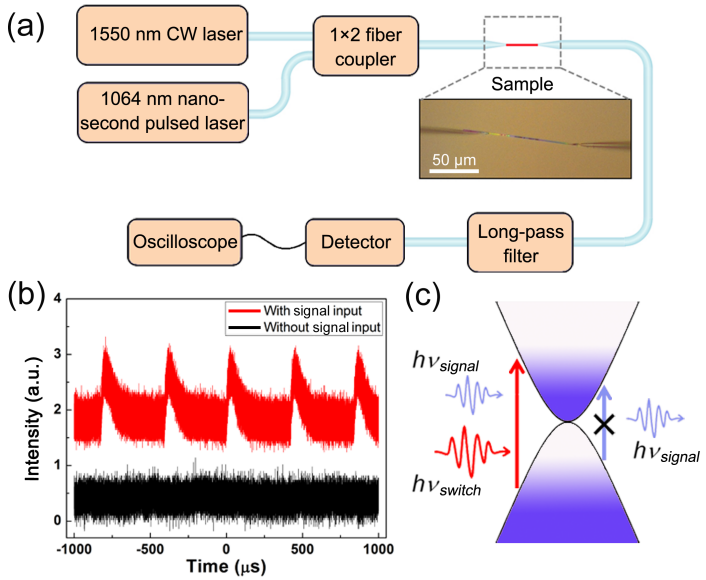

Fig. 5. Optical modulation based on a 590-nm-diameter GZN. (a) Schematic diagram of the modulation setup. (b) Pulses switched out from a 1550-nm CW beam in the GZN by an 8-ns 1064-nm pump pulse train (red curve). When the CW beam was removed from the setup, the modulated signal disappeared (black curve). The modulated signal curve was moved up vertically for demonstration clarity. (c) Schematic describes pump and probe of carriers in the valence and conduction bands of few-layer graphene. Excited carriers can lead to the band-filling effect that reduces the absorption of the CW signal light.

6. Conclusions

In summary, freestanding GZN optical waveguides were fabricated using a tape-assist transfer under micromanipulation. The graphene-induced propagation loss coefficient at 1550 nm was measured, indicating strong graphene-light interaction. Using femto-second pulses (1064- and 1550-nm wavelength, respectively), evident SA effects were observed in a 24-μm-length 475-nm-diameter GZN with a threshold peak power of 1.3 W. GZN-based optical modulation was also demonstrated, revealing the potential application in nonlinear nanophotonic devices. Also, the great versatility of available bandgaps of semiconductor NWs (ranging from violet to mid-IR) [29,33], which matches well with the ultra-broadband optical response of graphene, may offer a novel nanoscale platform for studying the graphene-light interaction in forms of graphene-functionalized NW waveguides, as well as a variety of technological applications in constructing nonlinear optical devices with miniaturized footprints.

#221151 - $15.00 USD Received 18 Aug 2014; revised 18 Sep 2014; accepted 18 Sep 2014; published 25 Sep 2014

Acknowledgments

This work was supported by the National Key Basic Research Program of China under Grant Agreement 2013CB328703, the National Natural Science Foundation of China under Grant Agreement 61108048, and the Fundamental Research Funds for the Central Universities under Grant Agreement 2013QNA5005. The authors thank Siyu Gong for Raman characterization and Yao Xiao for helpful discussions.

#221151 - $15.00 USD Received 18 Aug 2014; revised 18 Sep 2014; accepted 18 Sep 2014; published 25 Sep 2014